Research Square

Preprints are preliminary reports that have not undergone peer review.
They should not be considered conclusive, used to inform clinical practice,
or referenced by the media as validated information.

Research on dynamic characteristics of the point-the-bit rotary steering tool based on the multi-body system transfer matrix method

Hong Zhang
Yangtze University
Jiangxu Zhou
Yangtze University
Ding Feng
fengd08610163.com
Yangtze University
Kuo Liu
Ministry of Natural Resources
Yaojun Lin
Jingzhou shiji Paichuang Petroleum Machinery Testing CoLtd

Research Article

Keywords: Point-the-bit rotary steering tool, MSTMM, Spindle, Dynamic characteristics

Posted Date: May 5th, 2026

DOI: https://doi.org/10.21203/rs.3.rs-9376960/v1

License: This work is licensed under a Creative Commons Attribution 4.0 International License.
Read Full License

Additional Declarations: No competing interests reported.

Research on dynamic characteristics of the point-the-bit rotary steering tool based on the multi-body system transfer matrix method

Hong Zhang[1], Jiangxu Zhou[1], Ding Feng[1]✉, Kuo Liu[2], Yaojun Lin[3]

（[1]School of Mechanical Engineering,Yangtze University,Jingzhou,434023,China.[2]Technology Innovation Center for Directional Drilling Engineering, Ministry of Natural Resources,Langfang,065000,China.[3]Jingzhou shiji Paichuang Petroleum Machinery Testing CoLtd,Jingzhou,434000,China.✉email: fengd0861@163.com.）

Abstract: In the application of wellbore trajectory control, the dynamic characteristics of the spindle of the point-the-bit rotary steering tool are one of the decisive factors for the working characteristics and reliability of the spindle system. Under drilling conditions, the spindle's dynamic characteristics are affected by rotational speed, eccentricity and the installation position of the weight-on-bit (WOB) transmission mechanism. The multi-body system transfer matrix method (MSTMM) is adopted to establish the dynamic model of the tool's shell-bearing-spindle system, so as to study these factors' influences. By deriving the geometric and mechanical equations of any node on the spindle, their effects on the spindle's dynamic characteristics and the tool's well deviation building ability are evaluated, and the offset of the spindle's measuring points under different factors is calculated. To verify the model, an indoor bench test is conducted, whose results show that the experimental data basically coincide with the theoretical data, with a maximum offset error of only 6.48%, verifying the model's validity. Simultaneously a local model is established, and the discrete time transfer matrix method is used to derive its dynamic model. Case analysis shows that this method has a 95% curve fitting degree and a maximum error of 1.619 mm with the traditional finite element method, confirming its correctness. Further discussion indicates that the tool's lateral and torsional vibration frequencies are lower at medium speeds but increase sharply at low and high speeds, and rise slightly with increasing WOB and biasing force, without significant stability changes when biasing force varies.

Keywords: Point-the-bit rotary steering tool,MSTMM,Spindle,Dynamic characteristics

1 Introduction

The point-the-bit rotary steering tool is a key tool for implementing complex drilling technologies, used for controlling the wellbore trajectory[1–2]. This article discusses the challenges faced in China in the development of complex deep wells and how to address them[3]. In complex downhole environments, the spindle is subjected to multiple dynamic loads including torque, stick-slip vibrations, and drilling fluid disturbances. Such conditions are prone to trigger vibrational instabilities, leading to deviations in toolface angle control. This may even result in fatigue wear of critical components, compromising the long-term reliability of the tool under high-temperature, high-pressure conditions.In the case of point-the-bit rotary steering tools controlling wellbore trajectory, the spindle plays a vital role. Its dynamic characteristics are one of the decisive factors for the working characteristics and reliability of the entire drilling system[4]. In recent years, domestic research on the spindles of the point-the-bit rotary steering tools has not considered factors such as the interaction between the spindle and the housing, and the axial load acting on the spindle. However, these factors can affect the research and calculations under complex well conditions. Therefore, it is necessary to establish a dynamic model that takes these factors into account to conduct in-depth research on the dynamic characteristics of the spindle of the directional rotating steering tool. Currently, domestic research on the dynamic characteristics of directional rotating steering tool spindles is still limited[5–8]. For example, research has started late, and there are many key technical challenges. To analyze the dynamic behavior of the spindle caused by changes in spindle speed, WOB, and eccentric distance of the eccentric mechanism, Ding Feng and others[9–10] simplified the spindle of the directional rotating steering tool based on actual working conditions and used dynamic finite element analysis for calculations. Zhang Guangwei and others[11–13], based on finite element analysis, established a dynamic model of the guide shaft of the directional rotating steering tool and studied the effects of guide shaft deflection angle, torque, and WOB on the vibration characteristics of the guide shaft. Wu Qian and others[14] used dynamic theory and the energy method to establish a dynamic model of the spindle system of the directional rotating steering tool and explored the impact of eccentric distance on the longitudinal impact vibration characteristics of the spindle system. Tian Weikang[15] used the transfer matrix method and elastic dynamics to establish a dynamic model of the guide shaft and studied the natural frequency of the lateral vibration of the guide shaft.In summary, domestic research on the dynamic characteristics of the spindles of directional rotating steering tools generally uses methods such as finite element analysis, energy methods, and transfer matrix methods. Finite element modeling is complex and requires remodelling due to environmental changes,moreover, the computational difficulty increases exponentially with the number of degrees of freedom[16]. Theenergy method has long solution times and low efficiency, while The Multibody System Transfer Matrix Method (MSTMM) is well-suited for chain-type structures, utilizes low-order matrices, and efficiently handles rotating machinery problems.[17–18]Currently, research on applying the MSTMM to the dynamics of

multibody systems in rotary steerable drilling tools remains at a nascent stage.To further study the effects of the rotating steering tool housing, rotational speed, eccentricity and WOB transmission mechanism on the dynamic characteristics of the spindle, a multi-body system transfer matrix method was used to establish the dynamic model of the tool housing-bearing-spindle system. The model was analyzed for its dynamic characteristics, and the effects of rotational speed, eccentricity and the installation position of the WOB transmission mechanism on the dynamic characteristics of the spindle were explored. The correctness of the dynamic model was verified through example analysis,This provides an efficient computational approach for analyzing the dynamic response and steering capability of point-the-bit rotary steerable drilling tools. To further investigate the influences of rotational speed, WOB, and biasing force on the transient dynamic characteristics of the tool, a dynamic model of the point-the-bit rotary steering tool is established using the MSTMM. The dynamic response of the tool is obtained through solution. By comparing the lateral displacement of the steering tool with the results from Di Qinfeng's team using the finite element method (FEM), the validity of the discrete-time transfer matrix method is verified. Finally, the effects of rotational speed, weight on bit, and biasing force on the torsional and lateral vibration characteristics of the steering tool are discussed, providing a theoretical basis for the design and application of point-the-bit rotary steering tools,provide the theoretical basis for the design and application of point-the-bit rotary steering drilling tools.

2 Establishment of the Steady-State Dynamic Model

As outlined above, the research approach is presented in Fig.1.

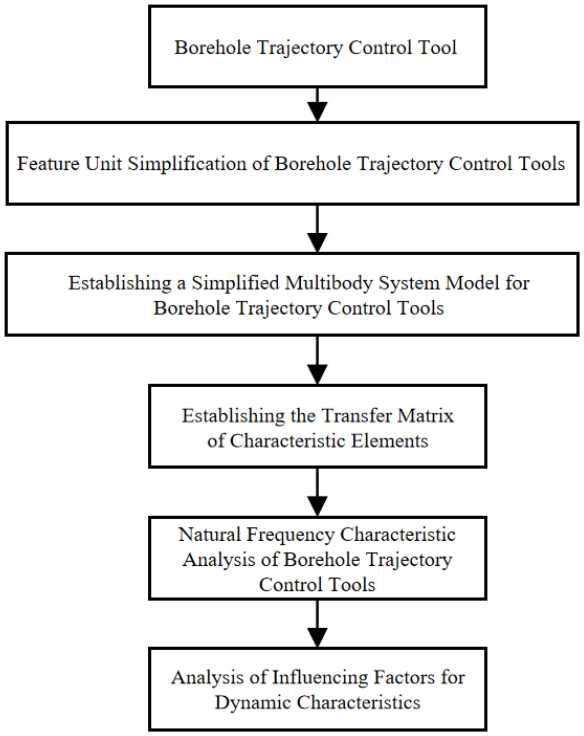


Fig.1 Research flowchart

In drilling operations, the directional rotating steering tool is used to ensure that the wellbore is drilled in the desired direction. An important component of this tool is the thrust bearing, which transfers the weight of the reactive force from the formation acting on the drill bit to the housing, preventing the spindle control section (composed of the lower and upper support bearings) from bearing axial loads. By avoiding the impact of axial loads on these bearings[19], the operation of the drilling tool becomes smoother and more efficient, leading to more successful drilling operations.The structure of the directional rotating steering tool is shown in Fig.2.

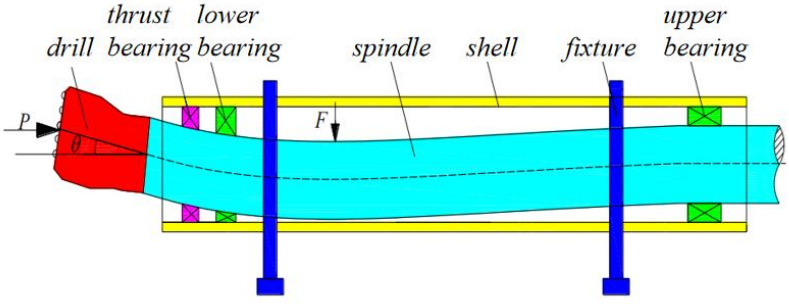


Fig.2 Structure diagram of Point-the-bit rotary steering tool

2.1 Establishment of the Steady-State Dynamic Model

This paper comprehensively considers the effects of axial loads, housing, eccentric mechanisms, WOB transmission mechanisms, and upper and lower support bearings. Fig.3 shows the dynamic model of the directional rotating steering tool system established using the multi-body system transfer matrix method. In the model, I represents the spindle, II represents the housing, F_1 and F_2 represent the biasing forces applied to the spindle and housing by the eccentric mechanism[20], K_r and K_θ are the radial stiffness and rotational stiffness of the housing and clamping mechanism, and K_c and K_{ch} represent the radial stiffness and rotational stiffness of the coupling bearings.

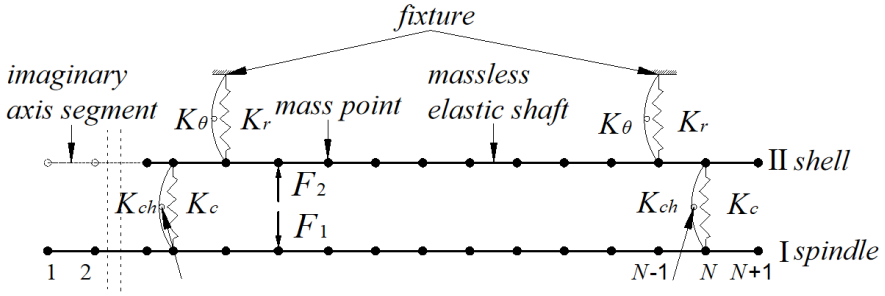


Fig.3 Housing-bearing-spindle system dynamics model

Let the state vector of any node **i** on the spindle and housing be defined as:

$$\begin{cases} \mathrm{Z}_i^{\mathrm{I}} = \begin{bmatrix} Y^{\mathrm{I}} & \theta^{\mathrm{I}} & M^{\mathrm{I}} & Q^{\mathrm{I}} \end{bmatrix}^T \\ \mathrm{Z}_i^{\mathrm{II}} = \begin{bmatrix} Y^{\mathrm{II}} & \theta^{\mathrm{II}} & M^{\mathrm{II}} & Q^{\mathrm{II}} \end{bmatrix}^T \end{cases} \tag{1}$$

Where Y is the deflection (in meters), θ is the rotational angle (in radians), M is the bending moment (in N·m), Q is the shear force (in N).

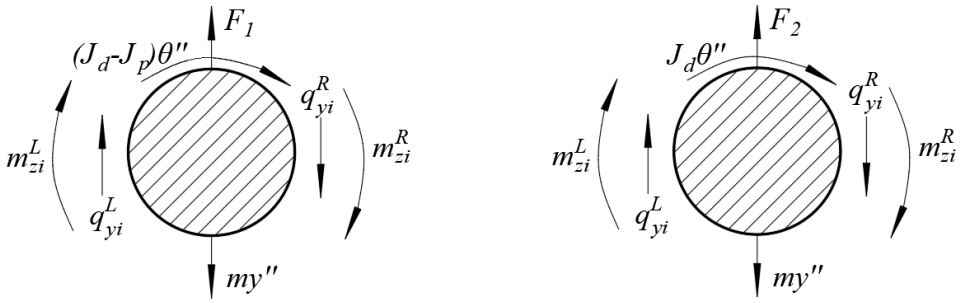
By integrating the state vectors of the spindle and housing into a single vector, the extended state vector of the overall transfer matrix can be obtained.

$$\mathrm{Z}_i = \begin{bmatrix} \mathrm{Z}_i^{\mathrm{I}} & 1 & \mathrm{Z}_i^{\mathrm{II}} & 1 \end{bmatrix}^T \tag{2}$$

In this context, "1" indicates the non-homogeneous terms (external forces) and the constants introduced by numerical methods.

The concentrated mass point element has only mass properties and no length properties. Therefore, the deflection and angular displacement at both ends of the concentrated mass point element are equal. For the force analysis of the concentrated mass point element on the spindle, it is assumed that the only external force acting on the concentrated mass point element **i** is the biasing force, and the effect of the gyroscopic torque is also considered.

Based on the mechanical equilibrium conditions and material mechanics theory[21], the mass point transfer matrix and the massless beam element transfer matrix for the spindle and housing can be derived. The transfer matrix form is shown below.



（a）Free-body diagram of the spindle shaft lumped mass

（b）Free-body diagram of the housing lumped mass

Fig.4 Force analysis of concentrated mass points

spindle

$$\begin{cases} y_i^R = y_i^L \\ \theta_i^R = \theta_i^L \\ m_i^R = m_i^L + \left(J_P - J_d\right)\omega^2\theta_i^L \\ q_i^R = q_i^L + m\omega^2 y_i^L + F_1 \end{cases}$$

shell

$$\begin{cases} y_i^R = y_i^L \\ \theta_i^R = \theta_i^L \\ m_i^R = m_i^L - J_d\omega^2\theta_i^L \\ q_i^R = q_i^L + m\omega^2 y_i^L + F_2 \end{cases}$$

The transfer equation for the spindle shaft lumped mass element is given as follows:

$$\begin{cases} Y_i^R = Y_i^L \\ \Theta_i^R = \Theta_i^L \\ M_i^R = M_i^L + (J_P - J_d)\omega^2\Theta_i^L \\ Q_i^R = Q_i^L + m\omega^2 Y_i^L + F_1 \end{cases} \Rightarrow \begin{bmatrix} Y \\ \Theta \\ M \\ Q \end{bmatrix}_R = \begin{bmatrix} 1 & 0 & 0 & 0 \\ 0 & 1 & 0 & 0 \\ 0 & (J_p - J_d)\omega^2 & 1 & 0 \\ m\omega^2 & 0 & 0 & 1 \end{bmatrix} \begin{bmatrix} Y \\ \Theta \\ M \\ Q \end{bmatrix}_L + \begin{bmatrix} 0 \\ 0 \\ 0 \\ F_1 \end{bmatrix} \quad (3)$$

The above equation is expressed in the extended transfer matrix form as follows:

$$\begin{bmatrix} Y \\ \Theta \\ M \\ Q \\ 1 \end{bmatrix}_O = \begin{bmatrix} 1 & 0 & 0 & 0 & 0 \\ 0 & 1 & 0 & 0 & 0 \\ 0 & (J_p - J_d)\omega^2 & 1 & 0 & 0 \\ m\omega^2 & 0 & 0 & 1 & F \\ 0 & 0 & 0 & 0 & 1 \end{bmatrix}_i \begin{bmatrix} Y \\ \Theta \\ M \\ Q \\ 1 \end{bmatrix}_I \quad (4)$$

Spindle Mass Point Element Extended Transfer Matrix:

$$T_{pi}^{\ \mathrm{I}} = \begin{bmatrix} 1 & 0 & 0 & 0 & 0 \\ 0 & 1 & 0 & 0 & 0 \\ 0 & (J_p^{\ \mathrm{I}} - J_d^{\ \mathrm{I}})\omega^2 & 1 & 0 & 0 \\ m^{\mathrm{I}}\omega^2 & 0 & 0 & 1 & F_1 \\ 0 & 0 & 0 & 0 & 1 \end{bmatrix}_i^{\mathrm{I}} \quad (5)$$

Similarly, the housing mass point element extended transfer matrix can be derived.

$$T_{pi}^{\ \mathrm{II}} = \begin{bmatrix} 1 & 0 & 0 & 0 & 0 \\ 0 & 1 & 0 & 0 & 0 \\ 0 & -J_d^{\ \mathrm{II}}\omega^2 & 1 & 0 & 0 \\ m^{\mathrm{II}}\omega^2 & 0 & 0 & 1 & F_2 \\ 0 & 0 & 0 & 0 & 1 \end{bmatrix}_i^{\mathrm{II}} \quad (6)$$

When the directional rotating steering tool bear WOB,the planar lateral elastic vibration beam is mainly subjected to the WOB and the uniformly distributed external load q_w due to gravity. The length of this beam is L_i, and the bending stiffness is *EI*. The force analysis of the massless elastic beam elements of the guide tool spindle and housing is shown in the Fig.5.

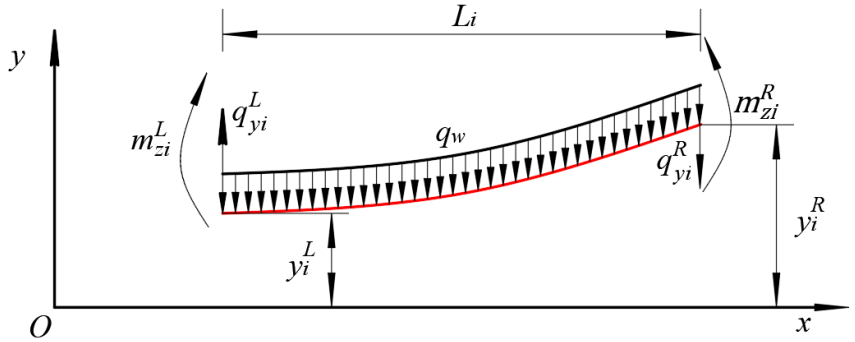


Fig.5 Force Analysis of Massless Elastic Beam Element under WOB Conditio

Under axial compressive load, the deflection, slope, bending moment, and shear force at the left (L) and right (R) ends of the beam are related by the following expression:

$$\begin{cases} y_i^{\,R} = y_i^{\,L} + \dfrac{\sinh(\lambda L)}{\lambda}\theta_{zi}^{\,L} - \dfrac{1-\cosh(\lambda L)}{d_1 EI} m_{zi}^{\,L} - \dfrac{\lambda L - \sinh(\lambda L) - \lambda L^3 v}{\lambda^3 EI} q_{zi}^{\,L} - \dfrac{q_{重} L^4}{24EI} \\ \theta_{zi}^{\,R} = \cosh(\lambda L)\theta_{zi}^{\,L} + \dfrac{\sinh(\lambda L)}{\lambda EI} m_{zi}^{\,L} - \dfrac{1-\cosh(\lambda L)}{d_1 EI} q_{zi}^{\,L} - \dfrac{q_{重} L^3}{6EI} \\ m_{zi}^{\,R} = \dfrac{d_1 EI \sinh(\lambda L)}{\lambda}\theta_{zi}^{\,L} + \cosh(\lambda L) m_{zi}^{\,L} + \dfrac{\sinh(\lambda L)}{\lambda} q_{yi}^{\,L} - \dfrac{q_{重} L^2}{2} \\ q_{yi}^{\,R} = d_1 EI \cosh(\lambda L)\theta_{zi}^{\,L} + \lambda \sinh(\lambda L) m_{zi}^{\,L} + \cosh(\lambda L) q_{yi}^{\,L} - q_{重} L \end{cases} \tag{7}$$

When the spindle or housing bear WOB , the extended transfer matrix for the massless beam element, considering shear deformation, is:

$$T_{fi}^{\,P} = \begin{bmatrix} 1 & \dfrac{\sinh\lambda L}{\lambda} & -\dfrac{1-\cosh\lambda L}{d_1 EI} & -\dfrac{\lambda L - \sinh\lambda L - \lambda L^3 v}{6\lambda EI} & -\dfrac{qL^4}{24EI} \\ 0 & \cosh\lambda L & \dfrac{\sinh\lambda L}{\lambda EI} & -\dfrac{1-\cosh\lambda L}{d_1 EI} & -\dfrac{qL^3}{6EI} \\ 0 & \dfrac{d_1 EI \sinh\lambda L}{\lambda} & \cosh\lambda L & \dfrac{\sinh\lambda L}{\lambda} & -\dfrac{qL^2}{2} \\ 0 & 0 & 0 & 1 & -qL \\ 0 & 0 & 0 & 0 & 1 \end{bmatrix} \tag{8}$$

According to the global transfer matrix method, spindle I and shell II need to meet the coordination condition through the coupling matrix at the coupling point, and the coupling point is set at node i. Mechanical analysis is performed on the coupling bearing at the node, as shown in Fig.6.The radial stiffness of the coupling bearing is K_c.The rotational stiffness of the coupling bearing is K_{ch}.

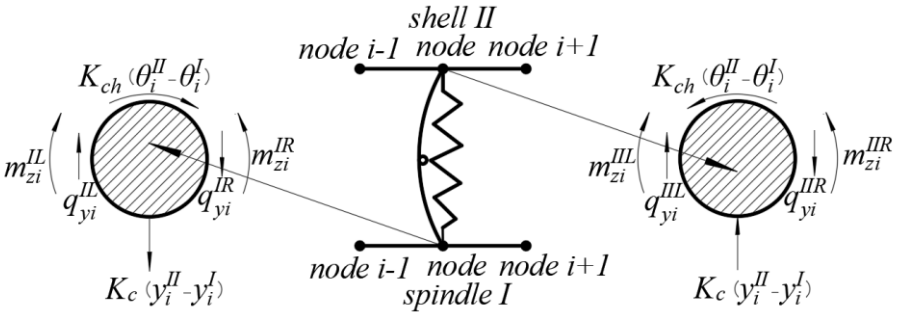


Fig.6 Force analysis of coupling bearing

According to the principle of force balance, the coordination equations of the two ends of the coupling between the spindle and the housing are listed:

spindle

$$\begin{cases} y_i^{\mathrm{I}R} = y_i^{\mathrm{I}L} \\ \theta_{zi}^{\mathrm{I}R} = \theta_{zi}^{\mathrm{I}L} \\ m_{zi}^{\ \mathrm{I}R} = m_{zi}^{\ \mathrm{I}L} + K_{ch}(\theta_{zi}^{\mathrm{II}} - \theta_{zi}^{\ \mathrm{I}}) \\ q_{zi}^{\ \mathrm{I}R} = q_{zi}^{\ \mathrm{I}L} + K_c(y_i^{\mathrm{I}} - y_i^{\mathrm{II}}) \end{cases}$$

shell

$$\begin{cases} y_i^{\mathrm{II}R} = y_i^{\mathrm{II}L} \\ \theta_{zi}^{\mathrm{II}R} = \theta_{zi}^{\mathrm{II}L} \\ m_{zi}^{\ \mathrm{II}R} = m_{zi}^{\ \mathrm{II}L} + K_{ch}(\theta_{zi}^{\mathrm{I}} - \theta_{zi}^{\ \mathrm{II}}) \\ q_{yi}^{\ \mathrm{II}R} = q_{yi}^{\mathrm{II}L} + K_c(y_i^{\mathrm{II}} - y_i^{\mathrm{I}}) \end{cases}$$

The transfer equation for the coupling bearings is formulated in the extended transfer matrix representation as follows:

$$\begin{bmatrix} Y^{\mathrm{I}} \\ \Theta^{\mathrm{I}} \\ M^{\mathrm{I}} \\ Q^{\mathrm{I}} \\ 1 \\ Y^{\mathrm{II}} \\ \Theta^{\mathrm{II}} \\ M^{\mathrm{II}} \\ Q^{\mathrm{II}} \\ 1 \end{bmatrix}_R = \begin{bmatrix} 1 & 0 & 0 & 0 & 0 & 0 & 0 & 0 & 0 & 0 \\ 0 & 1 & 0 & 0 & 0 & 0 & 0 & 0 & 0 & 0 \\ 0 & -K_{ch} & 1 & 0 & 0 & 0 & K_{ch} & 0 & 0 & 0 \\ K_c & 0 & 0 & 1 & 0 & -K_c & 0 & 0 & 0 & 0 \\ 0 & 0 & 0 & 0 & 1 & 0 & 0 & 0 & 0 & 0 \\ 0 & 0 & 0 & 0 & 0 & 1 & 0 & 0 & 0 & 0 \\ 0 & 0 & 0 & 0 & 0 & 0 & 1 & 0 & 0 & 0 \\ 0 & K_{ch} & 0 & 0 & 0 & 0 & -K_{ch} & 1 & 0 & 0 \\ -K_c & 0 & 0 & 0 & 0 & K_c & 0 & 0 & 1 & 0 \\ 0 & 0 & 0 & 0 & 0 & 0 & 0 & 0 & 0 & 1 \end{bmatrix} \begin{bmatrix} Y^{\mathrm{I}} \\ \Theta^{\mathrm{I}} \\ M^{\mathrm{I}} \\ Q^{\mathrm{I}} \\ 1 \\ Y^{\mathrm{II}} \\ \Theta^{\mathrm{II}} \\ M^{\mathrm{II}} \\ Q^{\mathrm{II}} \\ 1 \end{bmatrix}_L \tag{9}$$

At the upper and lower support bearings, the coupling matrix between the housing and spindle is as follows:

$$C_i = \begin{bmatrix} 1 & 0 & 0 & 0 & 0 & 0 & 0 & 0 & 0 & 0 \\ 0 & 1 & 0 & 0 & 0 & 0 & 0 & 0 & 0 & 0 \\ 0 & -K_{ch} & 1 & 0 & 0 & 0 & K_{ch} & 0 & 0 & 0 \\ K_c & 0 & 0 & 1 & 0 & -K_c & 0 & 0 & 0 & 0 \\ 0 & 0 & 0 & 0 & 1 & 0 & 0 & 0 & 0 & 0 \\ 0 & 0 & 0 & 0 & 0 & 1 & 0 & 0 & 0 & 0 \\ 0 & 0 & 0 & 0 & 0 & 0 & 1 & 0 & 0 & 0 \\ 0 & K_{ch} & 0 & 0 & 0 & 0 & -K_{ch} & 1 & 0 & 0 \\ -K_c & 0 & 0 & 0 & 0 & K_c & 0 & 0 & 1 & 0 \\ 0 & 0 & 0 & 0 & 0 & 0 & 0 & 0 & 0 & 1 \end{bmatrix} \tag{10}$$

Since the clamping mechanism mainly plays a supporting role in the test bench of the directional rotary steerable tool, it is equivalent to a supporting element, that is, the clamping mechanism can be regarded as a spring with both radial K_r and rotational stiffness K_θ, and the force analysis is carried out on it, as shown in Fig.7.

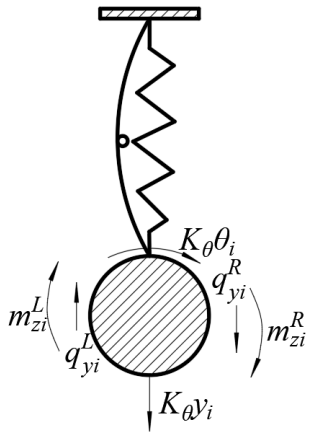


Fig.7 Force analysis diagram of support element

Based on the force equilibrium principle, the nodal compatibility equations at the coupling interface between the spindle shaft and housing are derived as follows:

$$\begin{cases} y_i^{\,R} = y_i^{\,L} \\ \theta_{zi}^{\,R} = \theta_{zi}^{\,L} \\ m_{zi}^{\,R} = m_{zi}^{\,L} + K_\theta \theta_i^{\,L} \\ q_{yi}^{\,R} = q_{yi}^{\,L} - K_r \mathrm{y}_i^{\,L} \end{cases} \tag{11}$$

The steady-state transfer matrix of the support element is:

$$T_J = \begin{bmatrix} 1 & 0 & 0 & 0 & 0 \\ 0 & 1 & 0 & 0 & 0 \\ 0 & K_\theta & 1 & 0 & 0 \\ -K_r & 0 & 0 & 1 & 0 \\ 0 & 0 & 0 & 0 & 1 \end{bmatrix} \tag{12}$$

In equations (3)–(10):

$\nu = \frac{6EI}{KGAL^2}, \lambda = \sqrt{\frac{P}{EI}}, d_1 = -\lambda^2,$

K is the shear deformation coefficient,

EI is the bending stiffness (N·m²),

GA is the shear stiffness (N·m²),

L is the length of the massless beam segment (m),

A is the cross-sectional area (m²),

F is the biasing force (N),

P is the WOB (N),

q is the uniformly distributed gravity load (N/m),

J_p is the polar moment of inertia (kg·m²),

J_d is the moment of inertia for diameter rotation (kg·m²),

K_r is the radial stiffness between the housing and clamping mechanism (N/m),

K_θ is the rotational stiffness between the housing and clamping mechanism (N·m/rad),

m is the concentrated mass (kg),

ω is the natural frequency (Hz),

K_c is the radial stiffness of the coupling bearing (N/m),

K_{ch} is the rotational stiffness of the coupling bearing (N·m/rad).

Using equations (2)–(10), the spindle mass—beam element transfer matrix $T_i^{\,\mathrm{I}}$ and the housing mass—beam element transfer matrix $T_i^{\,\mathrm{II}}$ can be obtained.

When the spindle is not under weight on bit

$$T_i^{\,\mathrm{I}} = T_{fi}^{\,\mathrm{I}} T_{pi}^{\,\mathrm{I}} \tag{13}$$

When the spindle is under weight on bit

$$T_i^{\,\mathrm{I}} = T_{fi}{}^{P\,\mathrm{I}} T_{pi}^{\,\mathrm{I}} \tag{14}$$

When the shell is not under weight on bit

$$T_i^{\,\mathrm{II}} = T_{fi}^{\,\mathrm{II}} T_{pi}^{\,\mathrm{II}} \tag{15}$$

When the shell is under weight on bit

$$T_i^{\,\mathrm{II}} = T_{fi}{}^{P\,\mathrm{II}} T_{pi}^{\,\mathrm{II}} \tag{16}$$

From the above, it is evident that in the housing-bearing-spindle system dynamic model, the overall state vector has the following transfer relationship:

$$Z_{i+1} = S_i Z_i = \begin{cases} T_i Z_i & uncoupled \\ C_i T_i Z_i & coupling \end{cases} \tag{17}$$

This matrix Si represents the combined transfer matrix of the entire system that links the spindle, housing, and bearings.$\mathrm{T_i} = \begin{bmatrix} \mathrm{T_i}^{\,\mathrm{I}} & 0 \\ 0 & \mathrm{T_i}^{\,\mathrm{II}} \end{bmatrix}$.

2.2 Calculation of Tool Critical Speed and Vibration Mode

In the housing-bearing-spindle system dynamic model, it is assumed that the state vectors of the spindle and housing nodes at both ends are the same. The first node of the tool is at the drill bit end, while the (N+1)th node is at the upper support bearing.

At the upper support bearing end, the condition remains fixed.

$$Z_{N+1} = [0^{I} \quad 0^{I} \quad M^{I} \quad Q^{I} \quad 1 \quad 0^{II} \quad 0^{II} \quad M^{II} \quad Q^{II} \quad 1]^{T}$$

Under drilling conditions, the drill bit end node is considered to be a hinged support.

$$Z_1 = [0^{I} \quad \theta^{I} \quad 0^{I} \quad Q^{I} \quad 1 \quad 0^{II} \quad \theta^{II} \quad 0^{II} \quad Q^{II} \quad 1]^{T}$$

The state vector between the first node and the (N+1)th node can be expressed by equation (17):

$$Z_{N+1} = SZ_1 \tag{18}$$

Where:$S = S_N S_{N-1} \cdots S_3 S_2 S_1$

By substituting the boundary conditions at both ends into equation (18), the characteristic equation can be obtained:

$$\begin{bmatrix} S_{1,2} & S_{1,4} & S_{1,7} & S_{1,9} \\ S_{2,2} & S_{2,4} & S_{2,7} & S_{2,9} \\ S_{6,2} & S_{6,4} & S_{6,7} & S_{6,9} \\ S_{7,2} & S_{7,4} & S_{7,7} & S_{7,9} \end{bmatrix} \begin{bmatrix} \theta^{I} \\ Q^{I} \\ \theta^{II} \\ Q^{II} \end{bmatrix} = - \begin{bmatrix} S_{1,5} + S_{1,10} \\ S_{2,5} + S_{2,10} \\ S_{6,5} + S_{6,10} \\ S_{7,5} + S_{7,10} \end{bmatrix} \tag{19}$$

In the equation, $S_{a,b}$ is the element of the matrix S at row a and column b .

By setting the axial load *P*, biasing force *F*, and uniformly distributed gravity load q to zero, the characteristic determinant is:

$$\begin{vmatrix} S_{1,2} & S_{1,4} & S_{1,7} & S_{1,9} \\ S_{2,2} & S_{2,4} & S_{2,7} & S_{2,9} \\ S_{6,2} & S_{6,4} & S_{6,7} & S_{6,9} \\ S_{7,2} & S_{7,4} & S_{7,7} & S_{7,9} \end{vmatrix} = 0 \tag{20}$$

By solving the characteristic determinant (equation 20), the total natural frequencies and critical speeds of the drilling system are obtained. Substituting the obtained natural frequencies into equation (19) will give the state vector at the drill bit end. Finally, substituting the natural frequencies and state vectors into equation (18) will yield the tool vibration modes corresponding to the respective natural frequencies.

2.3 Dynamic behavior of the spindle

To analyze the dynamics of the spindle in the directional rotating steering tool housing-bearing-spindle system under biasing force during drilling conditions, the spindle speed is substituted into equation (19) for solution. This will yield the state vectors at node 1 (drill bit end): $\theta^{I}{}_1$, $Q^{I}{}_1$, $\theta^{II}{}_1$, $Q^{II}{}_1$. Thus, under drilling conditions, the displacement, rotation angle, bending moment, and shear force at any node i of the spindle are:

$$\begin{bmatrix} y_i^{I} \\ \theta_i^{I} \\ M_i^{I} \\ Q_i^{I} \end{bmatrix} = \begin{bmatrix} S_{1,2} & S_{1,4} & S_{1,7} & S_{1,9} \\ S_{2,2} & S_{2,4} & S_{2,7} & S_{2,9} \\ S_{3,2} & S_{3,4} & S_{3,7} & S_{3,9} \\ S_{4,2} & S_{4,4} & S_{4,7} & S_{4,9} \end{bmatrix} \begin{bmatrix} \theta^{I} \\ Q^{I} \\ \theta^{II} \\ Q^{II} \end{bmatrix} + \begin{bmatrix} S_{1,5} + S_{1,10} \\ S_{2,5} + S_{2,10} \\ S_{3,5} + S_{3,10} \\ S_{4,5} + S_{4,10} \end{bmatrix} \tag{21}$$

Using the above equations, the vibration amplitudes at each node of the spindle under different speeds and WOBs can be obtained.

2.4 Calculation and Analysis of Tool Natural Frequencies and Vibration Modes

By establishing a mechanical model, the natural frequencies and vibration modes of the directional rotating steering tool are calculated. The thrust bearing is used as the WOB transmission mechanism, moving between the drill bit (the first node) and the lower support bearing (the fifth node). The outer diameter of the tool housing is 180 mm, the inner diameter is 150 mm, and the total length is 2810 mm. The elastic modulus is 211 GPa, and the mass is 164 kg. The outer diameter of the tool spindle is 70 mm, the inner diameter is 40 mm, and the total length is 3485 mm. The elastic modulus is 195 GPa, and the mass is 62 kg.

This paper primarily analyzes the first three natural frequencies of the tool, with the specific division shown in Fig.8.

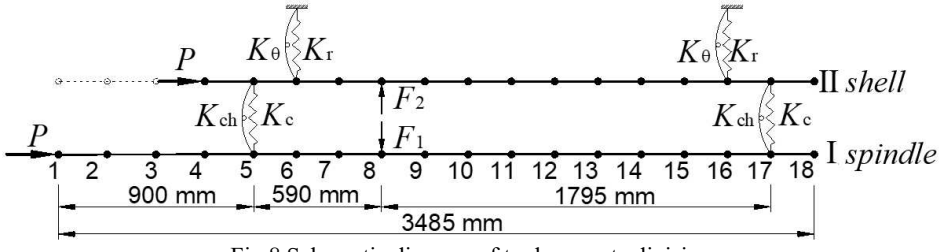


Fig.8 Schematic diagram of tool concrete division

By solving equation (20), the natural frequencies of the tool system under drilling conditions with an eccentricity of 6 mm and various WOB transmission mechanism installation positions at nodes 1, 2, 3, 4, and 5 are shown in Fig.9. From

the Fig, it can be observed that as the distance between the WOB transmission mechanism installation position and the drill bit increases, the natural frequencies continue to increase. Since the minimum natural frequency is 340.604 Hz, which is greater than the operating speed of the directional rotating steering tool (200 r/min), the tool spindle can operate safely and stably within this speed range without resonating.

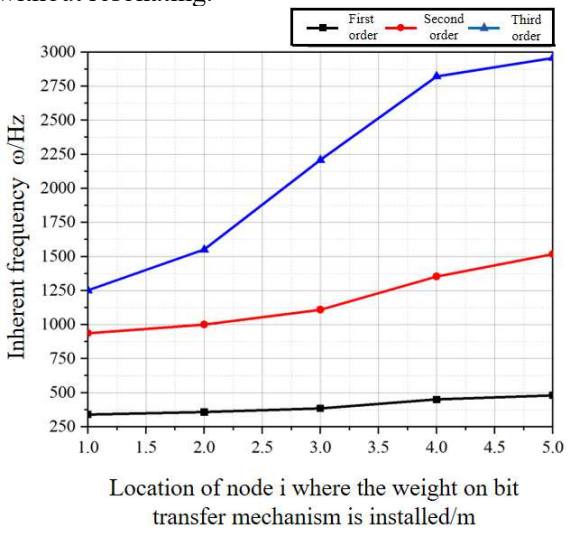
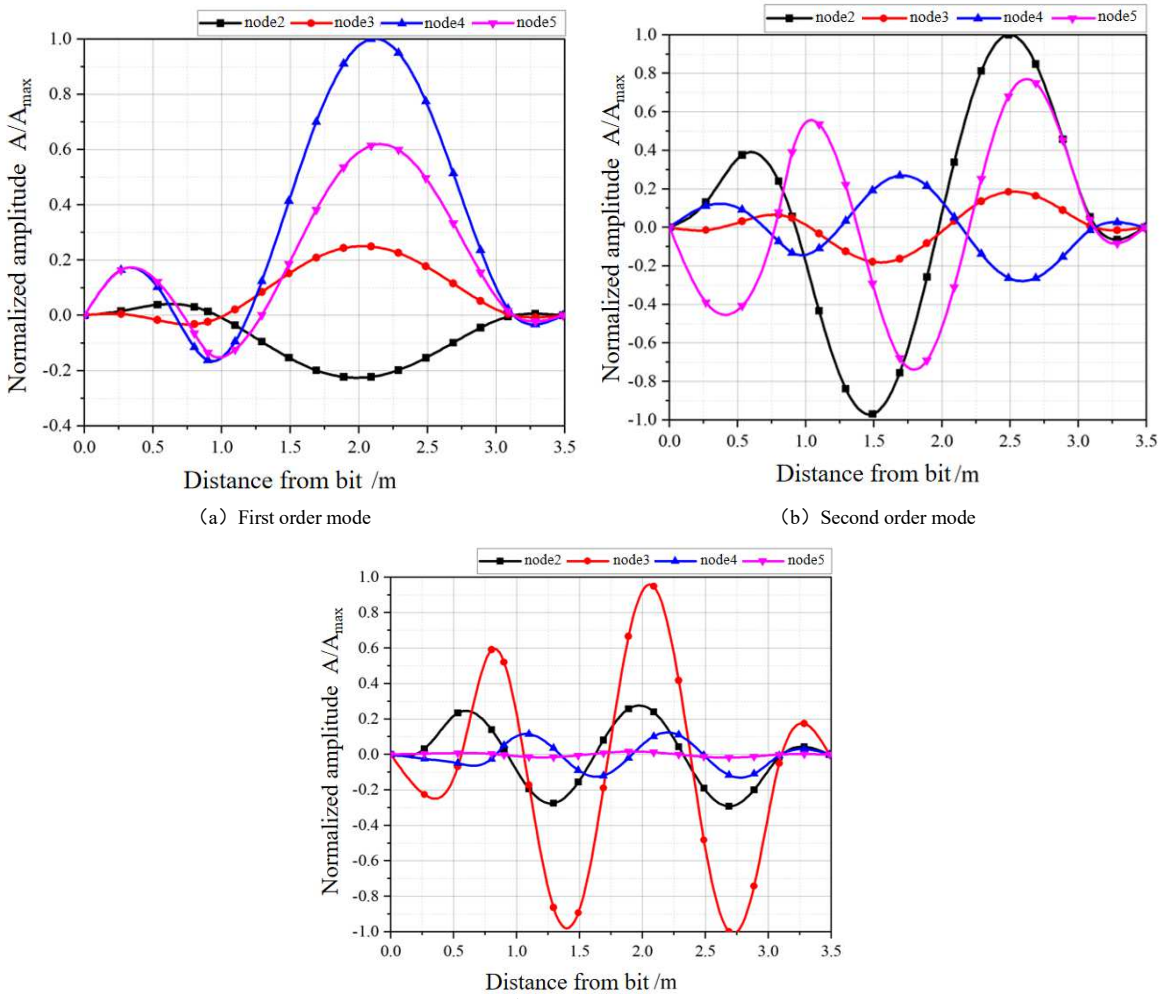


Fig.9 Influence of installation position of WOB transfer device on natural frequency of tool

Under drilling conditions with an eccentricity of 6 mm, the first three natural vibration modes of the spindle when the WOB transmission mechanism is installed at nodes 2, 3, 4, and 5 are shown in Fig.10. It can be seen that the first three vibration modes differ significantly.



（a）First order mode　　（b）Second order mode

（c）Third order mode

Fig.10 Influence law of the installation position of WOB transfer device on the first three modes of spindle

From the perspective of the directional rotating steering tool structure, as shown in Fig.10,node4 exhibits the maximum amplitude in the first-order mode,node 2 and node 5 exhibit the maximum amplitude in the second-order

mode,node3 exhibits the maximum amplitude in the third-order mode.the first three vibration modes have the following characteristics: The drill bit end of the guide spindle is in a hinged support state, and the upper support bearing end is fixed. The vibration amplitudes of the spindle at the drill bit and upper support bearing ends are zero. In the first three vibration modes, regardless of the installation position of the WOB transmission mechanism at any node, the maximum spindle vibration amplitude occurs between the offset mechanism and the upper support bearing. Additionally, in each vibration mode, as the distance between the WOB transmission mechanism installation position and the drill bit increases, the distance from the maximum spindle vibration amplitude to the drill bit also increases. For example, in the first and second vibration modes, the further the WOB transmission mechanism installation position is from the drill bit, the larger the spindle vibration amplitude becomes from the drill bit end to the lower support bearing end. Therefore, for field applications, to meet operational requirements, it is recommended that the WOB transmission mechanism be installed as close as possible to the drill bit end to reduce the spindle amplitude near the drill bit end.

3 Analysis of Influence Regularities on Spindle Dynamic Characteristics

(1)Impact Regularities of Spindle Speed and Eccentricity on Dynamic Characteristics

When investigating the influence regularities of spindle speed and eccentricity on dynamic displacement, a WOB of 10 kN was applied, and different spindle speeds and eccentricity values were input to analyze their effects.

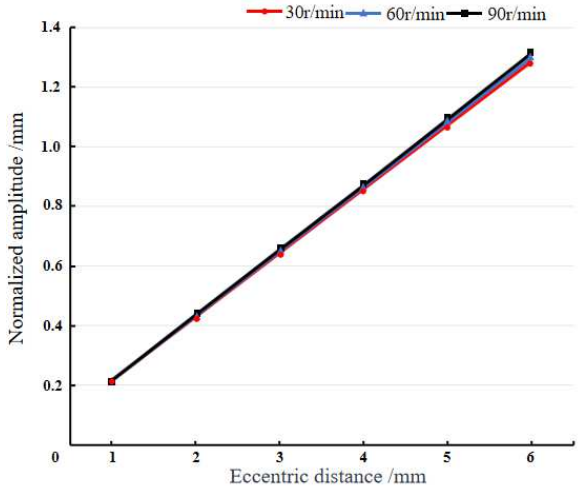


Fig.11 Effect of Rotational Speed and Eccentricity on the Dynamic Displacement of the Spindle

As shown in Fig.11, the spindle dynamic displacement exhibited minimal sensitivity to rotational speed under constant eccentricity. Although the spindle offset increased slightly with rising rotational speed, the maximum variation in dynamic displacement was only 0.002 mm. In contrast, the dynamic displacement demonstrated a proportional relationship with eccentricity, showing a significant upward trend as eccentricity increased.

(2)Influence Regularities of Installation Position of WOB Transmission Mechanism on Spindle Dynamic Characteristics.

When investigating the impact laws of the installation position of the WOB transmission mechanism on spindle dynamic displacement, experimental conditions were set at 60 r/min rotational speed, 6 mm eccentricity, and 10 kN WOB. The dynamic displacement characteristics were systematically analyzed under three installation configurations: Node 2, Node 3, and Node 4.

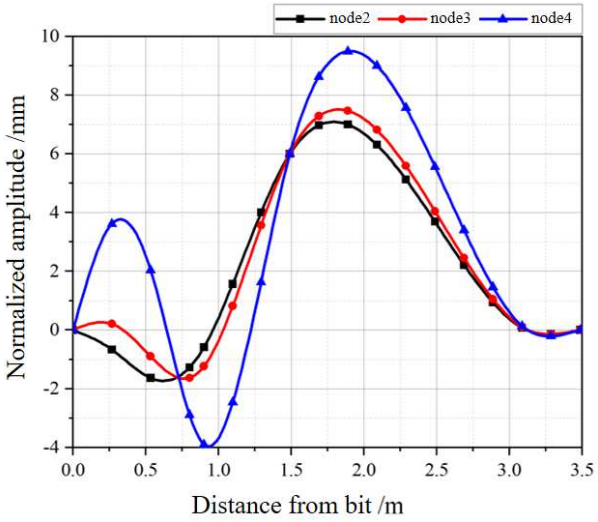


Fig.12 Influence law of installation position of WOB transfer device on dynamic displacement of spindle

As shown in Fig.12, under constant WOB, the dynamic displacement of the spindle increases as the installation position of the WOB transmission mechanism moves farther from the drill bit. Specifically:Drill bit end to lower support bearing section: The maximum discrepancy in dynamic displacement reaches 3.5 mm.Lower support bearing to offset mechanism section: A maximum dynamic displacement difference of 3.7 mm is observed.Offset mechanism to upper support bearing section: The dynamic displacement varies by up to 2.5 mm.

4 Experimental Verification

4.1 Analysis of Spindle Measurement Point Displacement

The principle of spindle measurement point displacement for the directional rotating steering tool is shown in Fig.13.

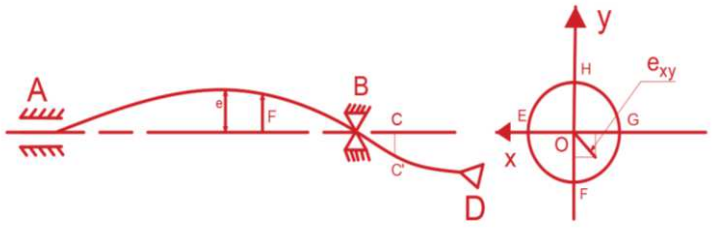


Fig.13 Test schematic

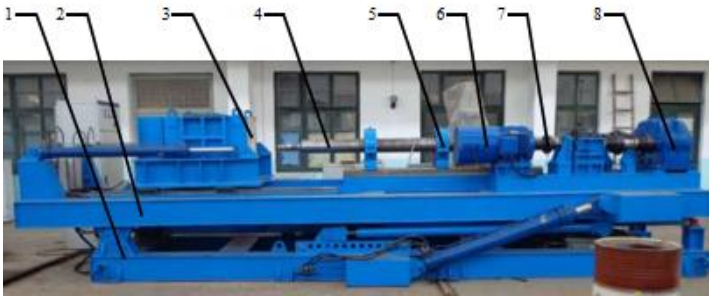
In this study, four eddy current displacement sensors were used. These sensors were placed at the C-C' cross-section of the spindle, corresponding to points E, F, G, and H on the outer diameter of the spindle, as shown in the Fig, to measure the displacement of the machine spindle. The sensors measured the deformation point C' at point C on the spindle and calculated the horizontal coordinates x_1, x_2 and vertical coordinates y_1, y_2. Based on these calculations, the combined displacement of the two lateral movements along the X and Y axes of the spindle section center, denoted as e_{xy}, was determined. The same method used for the C-C' section can be applied to measure the displacement at other required measurement nodes.

$$e_{xy} = \sqrt{(\frac{x_1 + x_2}{2})^2 + (\frac{y_1 + y_2}{2})^2} \quad (22)$$

4.2 Indoor Experiment

To verify the accuracy of the spindle dynamics model established using the transfer matrix method, as well as the impact of speed, eccentricity and WOB transmission mechanism installation position on the spindle dynamic displacement, a spindle measurement point displacement test experiment was conducted under drilling conditions on the test rig developed by the research team for the directional rotating steering tool, as shown in Fig.14. The test rig consists of a motor, guiding tool, and its clamping mechanism. The overall length of the rig is 8110 mm, width 1700 mm, and height 2300 mm.

Simulating drilling operations by penetrating a concrete block with a drill bit， the experiment verified the dynamics model and examined the effects of speed, eccentricity and the installation position of the WOB transmission mechanism on the spindle displacement. The experiment included altering speed, eccentricity and the installation position of the WOB transmission mechanism under drilling conditions, and measuring the spindle displacement with the displacement sensors. The results were processed and analyzed, and compared with the theoretical calculation results to verify the correctness of the established spindle dynamics model and the influence of speed, eccentricity and WOB transmission mechanism installation position on the spindle displacement.



1—Lower Frame Assembly;2—Upper Frame Assembly;3—Cement Test Block;4—Spindle;5—Clamping Device;6—Gear Reducer;7—Torque Sensor;8—Electric Motor

Fig.14 Point-the-bit rotary steering tool test bench

4.3 Experimental Results and Error Analysis of Spindle Measurement Point Displacement

(1)Analysis of Experimental Results on Spindle Speed and Eccentricity Effects on Measurement Point Displacement.

Dynamics Model Established Based on the Transfer Matrix Method.This section primarily calculates the spindle measurement point displacement. The spindle measurement point is located near the drill bit end, 100 mm away from the lower support bearing. For calculation convenience, it is set as spindle node 4, i.e., in Equation (17), where i=4,$S = S_2S_1$. When the directional rotating steering tool does not bear WOB, the spindle speeds of 30 r/min, 60 r/min, and 90 r/min are substituted into Equation (17) to obtain the spindle measurement point displacement y_3^{I} for different eccentricities.The experimental results, theoretical calculation results, and error analysis are summarized in Tab.1.

Tab.1 Test average results, theoretical result and error of measured point offset under no weight on bit conditions

The eccentricity of the inner and outer eccentric rings is synthesized（mm）	Experimental spindle speed 30 r/min offset of the measuring point（mm）	Theoretical spindle speed 30 r/min offset of the measuring point（mm）	Offset error of measuring point %	Experimental spindle speed 60 r/min offset of the measuring point（mm）	Theoretical spindle speed 60 r/min offset of the measuring point（mm）	Offset error of measuring point %	Experimental spindle speed 90 r/min offset of the measuring point（mm）	Theoretical spindle speed 90 r/min offset of the measuring point（mm）	Offset error of measuring point %
1	0.201	0.213	5.97	0.224	0.214	4.46	0.219	0.214	2.28
2	0.407	0.427	4.91	0.407	0.427	4.91	0.402	0.428	6.47
3	0.620	0.641	3.39	0.602	0.641	6.48	0.611	0.641	4.91
4	0.848	0.855	0.82	0.843	0.855	1.42	0.831	0.855	2.89
5	1.026	1.069	4.19	1.117	1.069	4.30	1.058	1.069	1.04
6	1.213	1.282	5.69	1.246	1.283	2.97	1.254	1.284	2.31

The experimental results indicate that the measured displacements at the spindle monitoring points demonstrate good agreement with theoretical calculations. For the investigation of rotational speed effects on spindle displacement, the maximum experimental error relative to theoretical values was measured at 0.039 mm, corresponding to a percentage error of 6.48%, which falls within acceptable engineering tolerances. Rotational speed exhibited negligible influence on spindle displacement. The maximum displacement deviation of 0.091 mm was observed under maximum eccentricity conditions (5 mm eccentricity). A direct proportional relationship was identified between eccentricity magnitude and spindle displacement magnitude, with displacement values increasing proportionally to eccentricity augmentation.

(2) Analysis of Experimental Results on the Influence of WOB Transmission Mechanism Mounting Position on Spindle Monitoring Point Displacement

In the dynamic model based on the transfer matrix method, the nodes are treated as mass points, and the remaining parts are considered as massless shafts. Since the WOB transmission mechanism is installed between the drill bit and the lower support bearing, the experiment only considers nodes 2, 3, and 4 as positions for the WOB transmission mechanism. To verify the accuracy of the simulation results, the spindle measurement points are set as follows: node 4 is positioned 100 mm from the lower support bearing in the segment from the drill bit to the lower support bearing (i=4), node 6 is located 197 mm from the lower support bearing in the segment from the lower support bearing to the offset mechanism (i=6), and node 10 is positioned 399 mm from the offset mechanism in the segment from the offset mechanism to the upper support bearing (i=10). To obtain the spindle measurement point displacement at different installation positions of the WOB transmission mechanism, the drilling conditions with a spindle speed of 60 r/min, WOB of 10 kN, and eccentricity of 6 mm are substituted into Equation (17). The experimental results, theoretical calculation results, and error analysis are summarized in Tab.2.

Tab.2 Test results, calculation results and error analysis of measured point offset under drilling conditions

Weight on bit transfer device installation position	Node4 experimental measuring point（mm）	Node4 calculated value（mm）	Node4 error(%)	Node6 experimental measuring point(mm)	Node6 calculated value（mm）	Node6 error(%)	Node10 experimental measuring point(mm)	Node10 calculated value（mm）	Node10 error(%)
Node2	1.314	1.276	2.97	1.594	1.572	1.42	7.306	7.005	4.30
Node3	1.687	1.632	3.39	0.864	0.811	6.13	7.829	7.463	4.91
Node4	2.717	2.889	5.97	2.356	2.459	4.19	9.769	9.495	2.89

The experimental results indicate that the spindle monitoring point displacement increases proportionally with the axial distance between the WOB transmission mechanism mounting position and the drill bit. Theoretical calculations and experimental measurements demonstrate high consistency, with a maximum deviation of 0.053 mm and a corresponding percentage error of 6.13%, both well within engineering tolerance requirements. This agreement validates the dynamic model established using the transfer matrix method and confirms the reliability of the research outcomes.

5 Establishment of the Transient Dynamic Model

The state vector of any node of rigid bodies and flexible bodies in the multi-body system of the point-the-bit rotary steering tool is:

$$\begin{cases} \boldsymbol{z}_i^{\,G} = \begin{bmatrix} x & y & z & \theta_x & \theta_y & \theta_z & m_x & m_y & m_z & q_x & q_y & q_z & 1 \end{bmatrix}^T \\ \boldsymbol{z}_i^{\,R} = \begin{bmatrix} x & y & z & \theta_x & \theta_y & \theta_z & m_x & m_y & m_z & q_x & q_y & q_z & q^1 & q^2 & q^3 & 1 \end{bmatrix}^T \end{cases} \tag{23}$$

In the formula, the superscript G represents the rigid bodies in the multi-body system of the steering tool, and the superscript R represents the flexible bodies in the multi-body system of the steering tool; *x, y,* and *z* are spatial coordinates, θ_x,θ_y and θ_z are angular displacements, m_x,m_y and m_z are internal moments, q_x,q_y and q_z are internal forces, and q^1, q^2, and q^3 are generalized modal coordinates.

$$\boldsymbol{z}_I = \begin{bmatrix} 0 & 0 & 0 & \theta_x & \theta_y & \theta_z & 0 & 0 & 0 & q_x & q_y & q_z & 1 \end{bmatrix}_I^T \tag{24}$$

Analyze output node *O* as a sliding fixed node, which can only perform translational motion along the x-axis and rotational motion about the x-axis, with its state vector defined as：

$$\boldsymbol{z}_O = \begin{bmatrix} x & 0 & 0 & \theta_x & 0 & 0 & 0 & m_y & m_z & 0 & q_y & q_z & q^1 & q^2 & q^3 & 1 \end{bmatrix}_O^T \tag{25}$$

Analyze the point-the-bit rotary steerable tool using the transient transfer matrix method, with its state vector defined as：

$$\boldsymbol{z}_O = \boldsymbol{U}_{R15}\boldsymbol{U}_{J14}\boldsymbol{U}_{G13}\boldsymbol{U}_{J12}\boldsymbol{U}_{R11}\boldsymbol{U}_{J10}\boldsymbol{U}_{R9}\boldsymbol{U}_{J8}\boldsymbol{U}_{R7}\boldsymbol{U}_{J6}\boldsymbol{U}_{G5}\boldsymbol{U}_{J4}\boldsymbol{U}_{R3}\boldsymbol{U}_{J2}\boldsymbol{U}_{G1} \cdot \boldsymbol{z}_I \tag{26}$$

In the equation, $\boldsymbol{U}_{\mathrm{Ri}}$ represents the transient transfer matrix of the flexible body; $\boldsymbol{U}_{\mathrm{Gi}}$ represents the transient transfer matrix of the rigid body; $\boldsymbol{U}_{\mathrm{Ji}}$ represents the transient transfer matrix of the fixed joint connecting the elements. The discrete-time transfer matrices of the aforementioned rigid bodies, flexible bodies, and fixed joints can be found in reference [15].

Rearranging Equation (26) yields the overall transfer equation of the multi-body system of the point-the-bit rotary steerable tool：

$$\boldsymbol{U}_{all}\boldsymbol{z}_{all} = O_{16\times1} \tag{27}$$

In the equation, $\boldsymbol{U}_{\mathrm{all}}$ is the overall transfer matrix of the steerable tool, and $\boldsymbol{z}_{all}$ is the state vector of the steerable tool, expressed by the following formula:

$$\boldsymbol{U}_{all} = \begin{bmatrix} \boldsymbol{U}_{R15}\boldsymbol{U}_{J14}\boldsymbol{U}_{G13}\boldsymbol{U}_{J12}\boldsymbol{U}_{R11}\boldsymbol{U}_{J10}\boldsymbol{U}_{R9}\boldsymbol{U}_{J8}\boldsymbol{U}_{R7}\boldsymbol{U}_{J6}\boldsymbol{U}_{G5}\boldsymbol{U}_{J4}\boldsymbol{U}_{R3}\boldsymbol{U}_{J2}\boldsymbol{U}_{G1} & -I_{16\times16} \end{bmatrix} \tag{28}$$

$$\boldsymbol{z}_{all} = \begin{bmatrix} \boldsymbol{z}_I^{\,T} & \boldsymbol{z}_O^{\,T} \end{bmatrix}^T \tag{29}$$

To obtain the unknown quantities in the state vectors of the boundary nodes in Equations (24) and (25), substitute the boundary conditions of the point-the-bit rotary steerable tool from Equations (24) and (25) into Equation (29) and rearrange to obtain the result.：

$$\overline{\boldsymbol{U}}_{\text{总}}\,\overline{\boldsymbol{z}}_{\text{总}} = -\boldsymbol{B} \tag{30}$$

In the equation, $\overline{\boldsymbol{z}}_{\text{总}}$ is the column matrix composed of unknown quantities extracted from $\boldsymbol{z}_{all}$, $\overline{\boldsymbol{U}}_{\text{总}}$ is the column matrix composed of unknown quantities extracted from $\boldsymbol{U}_{\mathrm{all}}$, and $\boldsymbol{U}_{\mathrm{i,\ j}}$ is the value of the element in the i-th row and j-th column of $\boldsymbol{U}_{\mathrm{all}}$

$$\boldsymbol{B} = \begin{bmatrix} U_{1,13} & U_{2,13} & U_{3,13} & U_{4,13} & U_{5,13} & U_{6,13} & U_{7,13} & U_{8,13} & U_{9,13} & U_{10,13} & U_{11,13} & U_{12,13} & U_{13,13} & U_{14,13} & U_{15,13} \end{bmatrix}^T$$

Solve the linear system of equations in Equation (30) to determine the state vectors at each node, thereby obtaining the dynamic response of the multi-body system of the point-the-bit rotary steerable tool.

6 Transient Example Calculation

Taking the data of Baker Hughes' AutoTrak tool as an example, the bit diameter is 216.9 mm, the rotary steerable tool diameter is 172 mm, the flexible sub outer diameter is 127 mm, the drill collar outer diameter is 172 mm and inner diameter is 71.4 mm, and the stabilizer outer diameter is 213 mm and inner diameter is 172 mm, as shown in Fig.15.

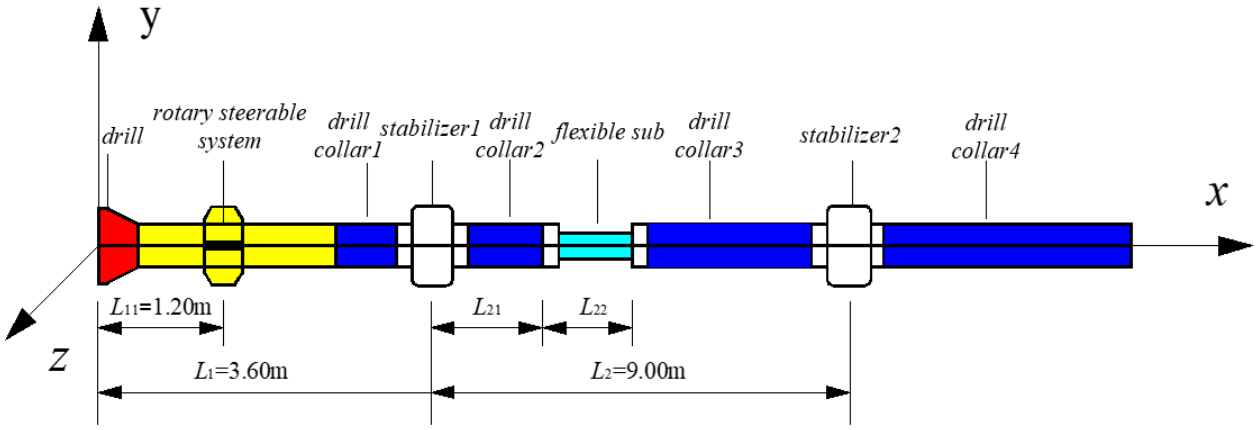
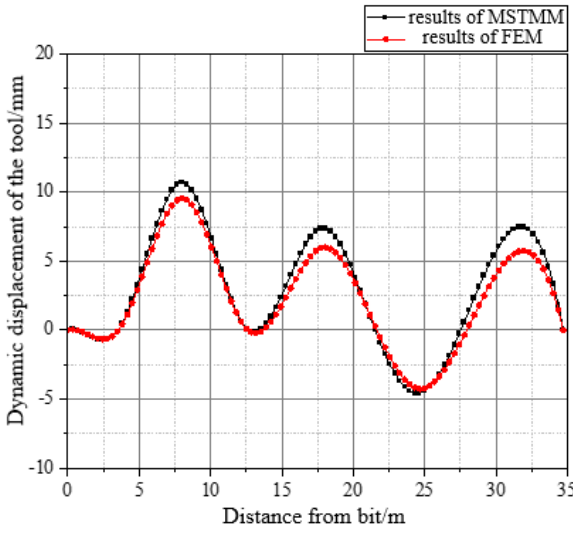
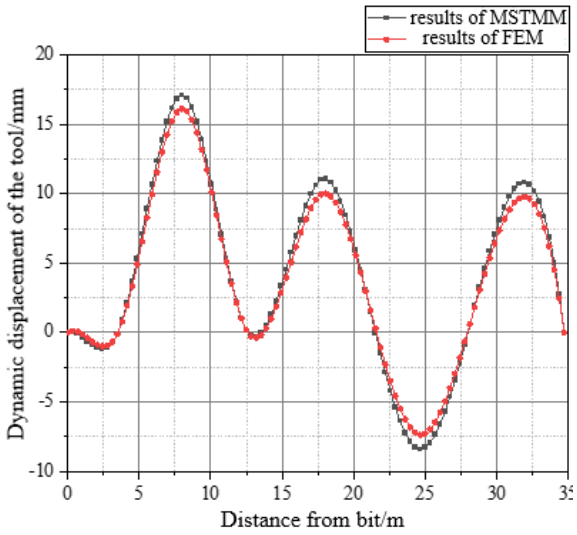


Fig.15 Simplified AutoTrak model

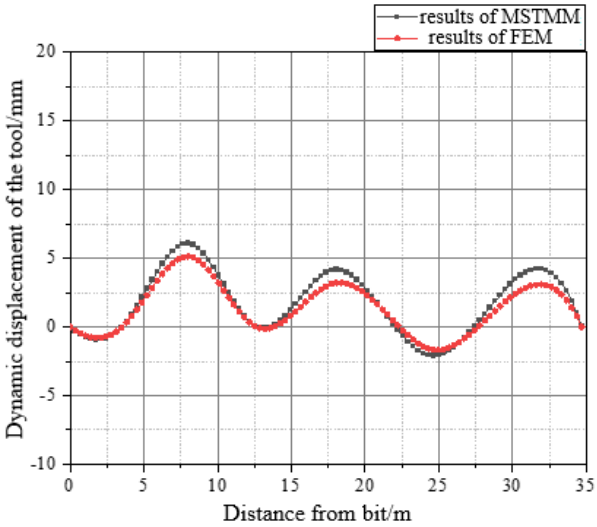
To verify the correctness of the discrete-time transfer matrix method, the average lateral dynamic displacement of the steerable tool at different rotational speeds is calculated using the above method and compared with the results obtained from the finite element method in reference [12]. When the weight on bit is 90 kN and the rotational speeds are 130 r/min, 140 r/min, and 150 r/min, the dynamic displacements from both methods are shown in Fig.16.



（a）Transverse Dynamic Displacement of RSBHA at 130r/min



（b）Transverse Dynamic Displacement of RSBHA at 140r/min



（c）Transverse Dynamic Displacement of RSBHA at 150r/min

Fig.16 Comparison of dynamic displacement of RSBHA

As shown in Fig.16, the lateral dynamic displacement obtained by the discrete-time transfer matrix method shows a 95% agreement with that obtained by the finite element method. However, at four points located 8.20 m, 18.10 m, 24.60 m, and 31.60 m from the bit, there are certain differences in dynamic displacement between the two methods. The maximum difference is 1.619 mm at the point 31.60 m from the bit at a rotational speed of 130 r/min, which is within the allowable error range required by engineering standards.

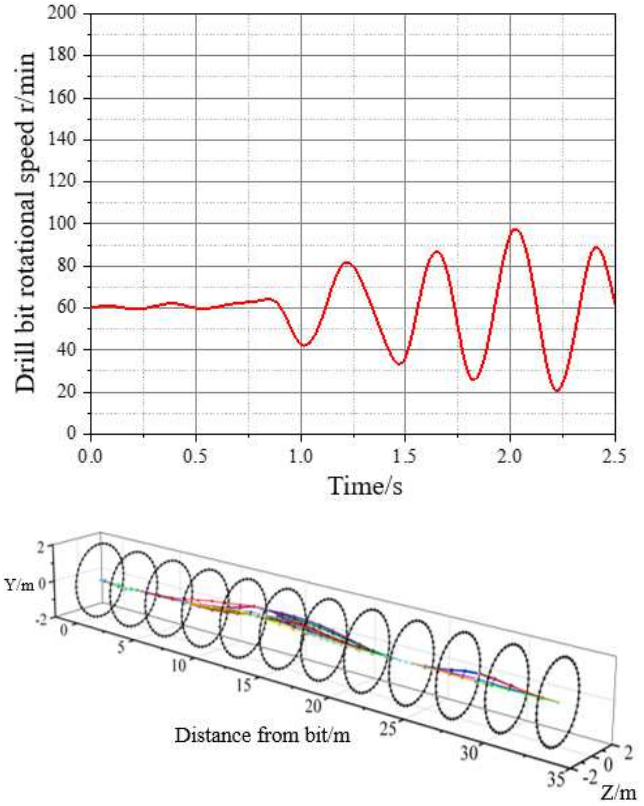
The point-the-bit rotary steerable tool has a large number of degrees of freedom. The computational cost of the finite element method increases exponentially with the number of degrees of freedom, greatly increasing the computational burden. In contrast, the discrete-time transfer matrix method does not require establishing the global dynamic equations of the system, features low matrix order, and has high computational efficiency. The small error between the two methods demonstrates the accuracy and efficiency of the discrete-time transfer matrix method.

7 Transient Dynamic Characteristic Analysis

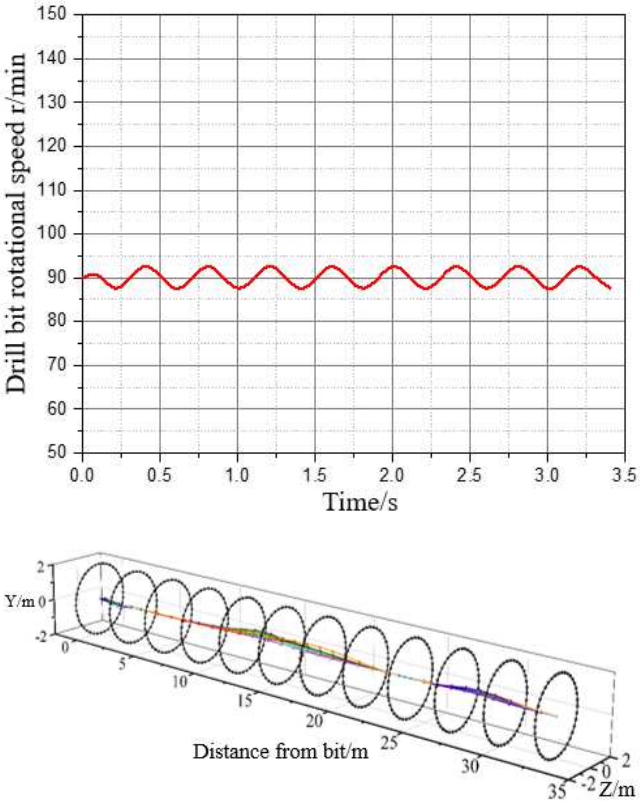
Substituting different initial conditions into Equation (30) yields the state vector z_I of node I. The angular displacement θ in z_I is linearized using the *Newmark-β* method to obtain the bit rotational speed, which is used as a representative to analyze the torsional vibration characteristics of the steerable tool. Then, z_I is substituted into the transient transfer matrix of each node to obtain the overall lateral displacement of the tool, and the overall lateral dynamic displacement of the steerable tool is used as a representative to analyze the lateral vibration characteristics.

(1)Impact Regularities of Speed on Tool Transient Dynamic Characteristics

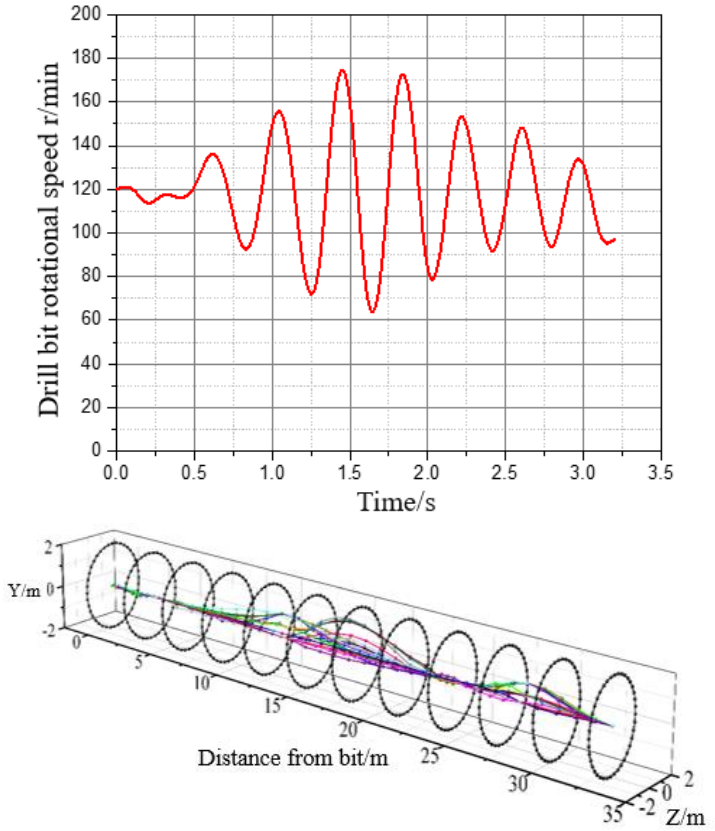
When the initial conditions of the point-the-bit rotary steerable tool are a bias force of 5 kN and a weight on bit of 60 kN, three different rotational speeds of 60 r/min, 90 r/min, and 120 r/min are input, and the bit rotational speed and lateral dynamic deformation of the point-the-bit rotary steerable tool at different rotational speeds are obtained, as shown in the figure below.



（a）Point-the-bit RSBHA dynamic characteristics when rotary speed is 60 r/min



（b）Point-the-bit RSBHA dynamic characteristics when rotary speed is 90 r/min



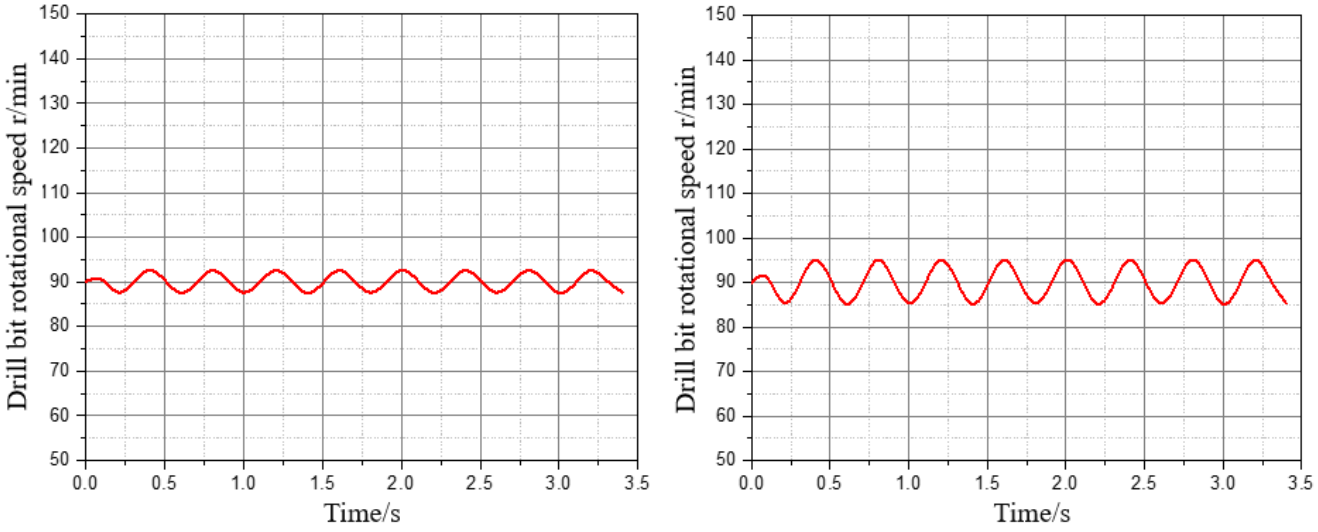
（c）Point-the-bit RSBHA dynamic characteristics when rotary speed is 120 r/min

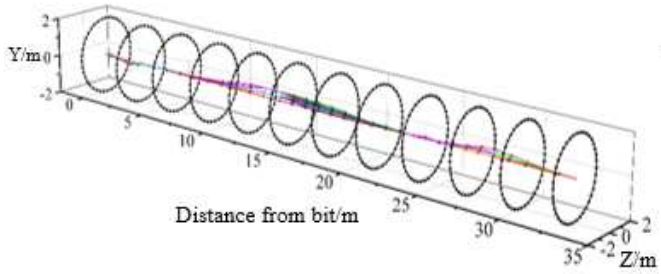
Fig.17 Dynamic characteristics of RSBHA under different rotational speed conditions

It can be observed from Fig.17(a) to 17(c) that the lateral displacement of the point-the-bit rotary steerable tool is significantly affected by changes in rotational speed, and different rotational speeds lead to different torsional vibrations of the bit. When the rotational speed of the point-the-bit rotary steerable tool is 60 r/min, the maximum fluctuation amplitude of the rotational speed is 78.5 r/min. When the rotational speed increases to 90 r/min, the torsional vibration amplitude decreases, with the maximum fluctuation amplitude of the rotational speed being 4.9 r/min. When the rotational speed increases to 120 r/min, the torsional vibration intensifies, with the maximum fluctuation amplitude of the rotational speed reaching 108.3 r/min. Therefore, during the operation of the point-the-bit rotary steerable tool, a rotational speed of around 90 r/min should be selected.

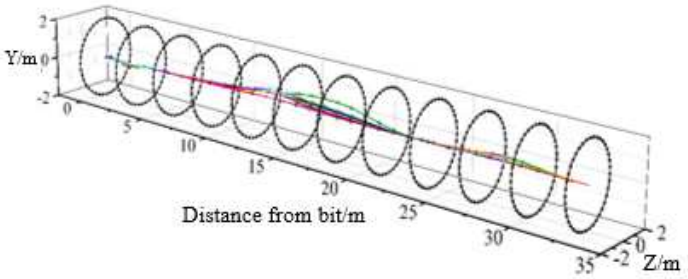
(2)Impact Regularities of WOB on Tool Transient Dynamic Characteristics

When the initial conditions of the point-the-bit rotary steerable tool are a rotational speed of 90 r/min and a bias force of 5 kN, three different weights on bit of 60 kN, 90 kN, and 120 kN are input, and the bit rotational speed and lateral dynamic deformation of the point-the-bit rotary steerable tool under different weights on bit are obtained, as shown in the figure below.

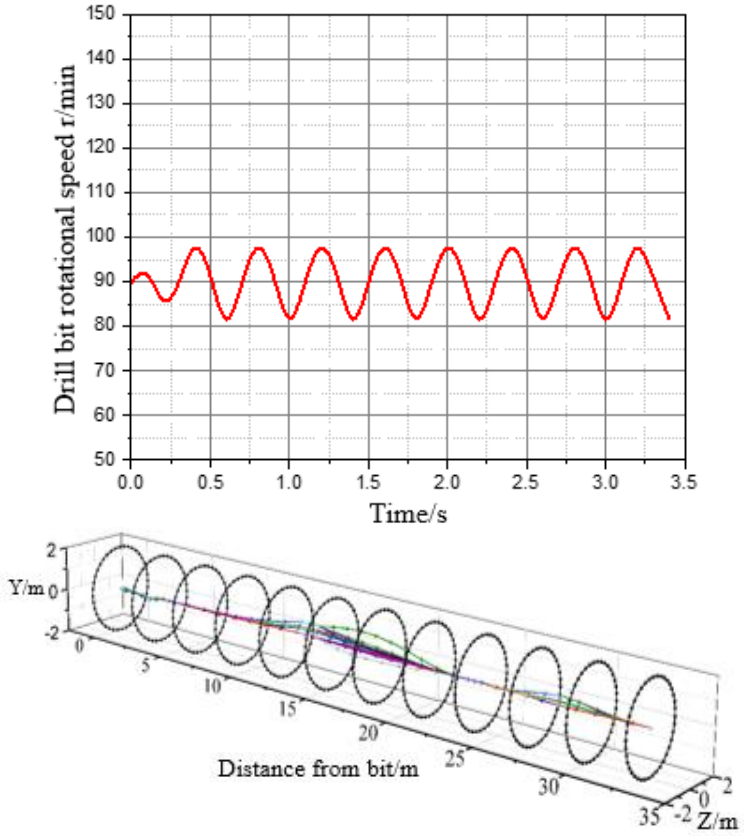




（a）Point-the-bit RSBHA dynamic characteristics when WOB is 60 kN



（b）Point-the-bit RSBHA dynamic characteristics whenWOB is 90 kN



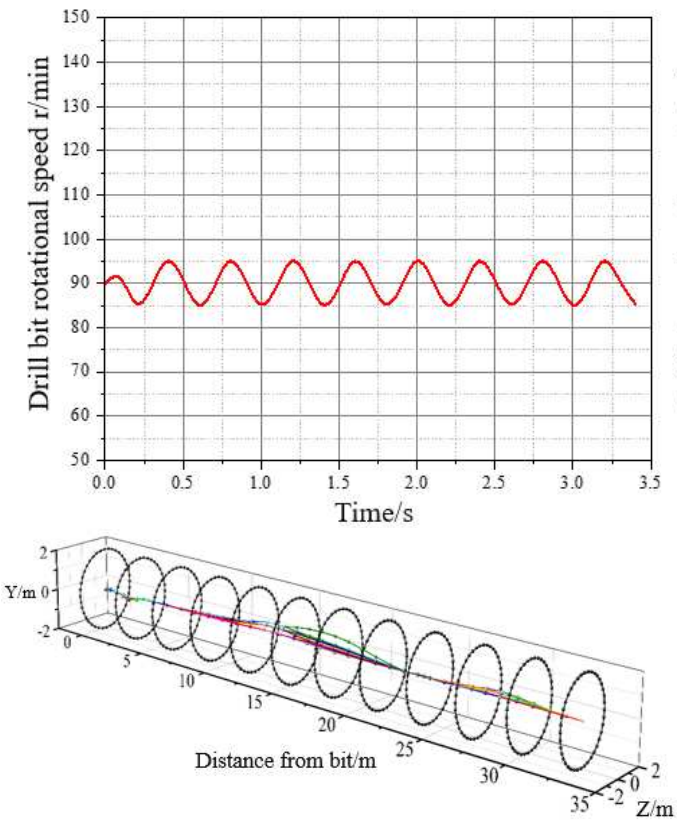
（c）Point-the-bit RSBHA dynamic characteristics when WOB is 120 kN

Fig.18 Dynamic characteristics of RSBHA under different WOB conditions

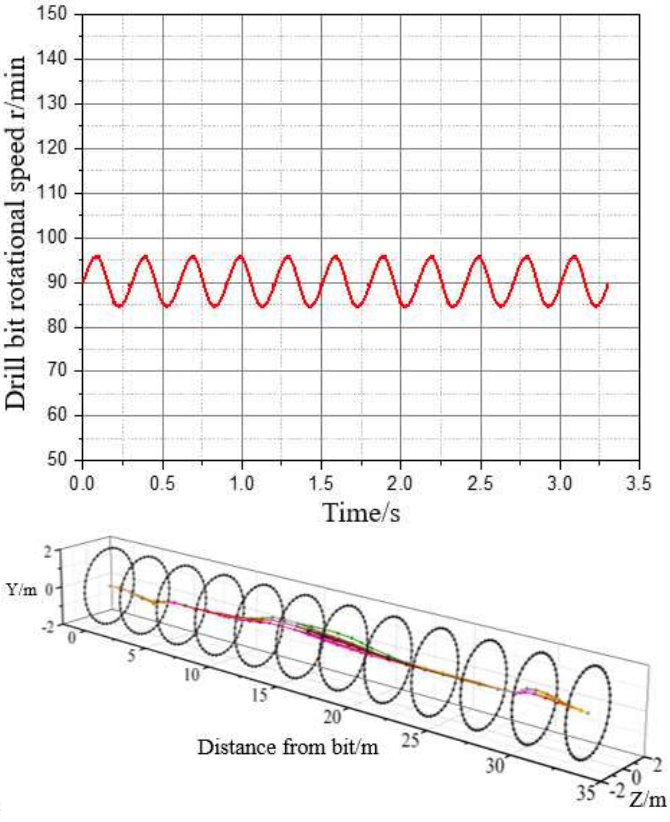
It can be observed from Fig.18(a) to 18(c) that the lateral displacement of the point-the-bit rotary steerable tool is less affected by changes in weight on bit, while the torsional vibration amplitude of the bit increases with the increase in weight on bit. When the weight on bit is 60 kN, the rotational speed fluctuation amplitude is 4.9 r/min; when the weight on bit increases to 90 kN, the fluctuation amplitude increases to 9.6 r/min; when the weight on bit increases to 120 kN, the fluctuation amplitude reaches 16 r/min. Therefore, during the operation of the point-the-bit rotary steerable tool, it is recommended to use a low weight on bit to reduce the torsional vibration of the bit.

(3)Impact Regularities of Biasing Force on Tool Transient Dynamic Characteristics

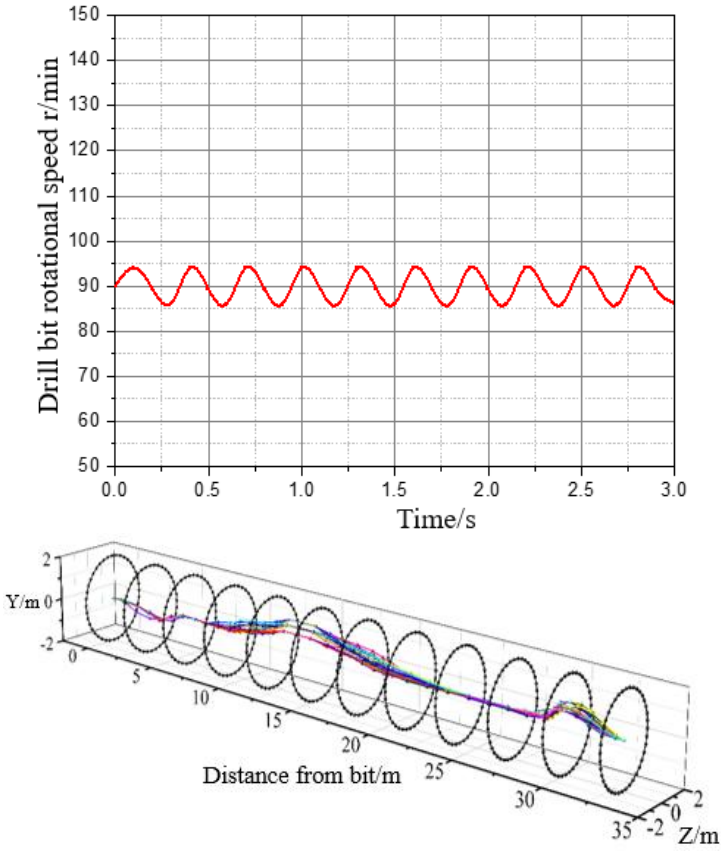
When the initial conditions of the point-the-bit rotary steerable tool are a rotational speed of 90 r/min and a weight on bit of 90 kN, three different bias forces of 5 kN, 10 kN, and 15 kN are input, and the bit rotational speed and lateral dynamic deformation of the point-the-bit rotary steerable tool under different bias forces are obtained, as shown in the figure below.



（a）Point-the-bit RSBHA dynamic characteristics when biasing force is 5 kN



（b）Point-the-bit RSBHA dynamic characteristics when biasing force is 10 kN



（c）Point-the-bit RSBHA dynamic characteristics when biasing force is 15 kN

Fig.19 Dynamic characteristics of RSBHA under different biasing force conditions

It can be observed from Fig.19(a) to 19(c) that the lateral displacement of the point-the-bit rotary steerable tool is less affected by changes in bias force, and its torsional vibration is also less affected by changes in bias force. When the

bias force is 5 kN, the rotational speed fluctuation amplitude is 9.6 r/min; when the bias force increases to 10 kN, the fluctuation amplitude is 10.2 r/min; when the bias force increases to 15 kN, the fluctuation amplitude is 8 r/min. Therefore, changing the magnitude of the bias force does not significantly alter the motion stability of the steerable tool.

Conclusion

（1）This paper established the dynamic model of the directional rotary steerable tool's outer casing-bearing-spindle system using the multi-body system transfer matrix method, providing a theoretical foundation for the analysis of tool vibration characteristics.

（2）The paper explored the influence of the installation position of the WOB transmission mechanism on the inherent frequencies of the directional rotary steerable tool. The results show that as the distance between the WOB transmission mechanism and the drill bit increases, the spindle's natural frequency increases. Specifically, the first-order natural frequency increases by 41.2%, the second-order by 62.2%, and the third-order by 136.5%. Since the spindle's rotation speed is lower than the first-order natural frequency, resonance is eliminated, ensuring the tool's stable operation.

（3）This study investigates the influence of rotational speed, eccentricity, and the installation position of the WOB transfer mechanism on the spindle's dynamic displacement in a pointing-type rotary steering tool. Through laboratory experimental validation, it was found that the deflection of the spindle measurement point during operation fundamentally aligns with theoretical calculations, with a maximum error of 0.039 mm ,the error rate is 6.48%, meeting engineering requirements. At an eccentricity of 5 mm, the maximum deviation error reached 0.091 mm.A proportional relationship was observed between spindle deflection and eccentricity: deflection increases with larger eccentricity values.Increasing the installation distance between the WOB transmission mechanism and the drill bit led to greater spindle deflection, with a peak error of 0.053 mm,the error rate is 6.13%.

（4）The influence laws of three factors, namely rotational speed, WOB and biasing force, on the torsional vibration and transverse vibration of the point-the-bit rotary steering tool were analyzed. The results show that the rotational speed of the steering tool should be around 90 r/min to reduce the transverse vibration and torsional vibration during tool operation; from the perspective of reducing the torsional vibration of the drill bit, it is recommended that the steering tool adopt low WOB drilling; the biasing force has little influence on the fluctuation amplitude of the torsional vibration of the drill bit and the transverse vibration of the steering tool.

Data Availability

The data supporting the findings of this study are fully available within the manuscript . Reasonable requests for further clarification can be directed to the corresponding author.

References

[1]Feng Ding, Wang Peng, Zhang Hong, et al. Development status and trend of well trajectory control tool [J]. China Petroleum Machinery, 2021, 49(07): 8-15.

[2]Zhang Hong, Shi Lei, Liu Xuhui, et al. Research on the Spindle Deflecting Reliability of the Wellbore Trajectory Control Tool Based on Palmgren-Miner[J]. Journal of Mechanical Science and Technology, 2020, 34 (12): 4925~4931.

[3]Hou Pengpeng. Research on steering principle and dynamic characteristics of full rotation closed loop pointing steering drill [D]. Xi'an Shiyou University,2021.

[4] Feng D, Wu L, Wang JW, et al. Research on eccentric dis-placement of the trajectory control tool of high build-up rate wellbore. Lecture Notes in In-formation Technology, 2012, 9: 291-296.

[5]Millheim K K, Apostal M C. 1981. The effect of bottom hole assembly dynamics on the trajectory of a bit. Journal of Petroleum Technology, 1981, 33: 2323-2338.

[6]Apostal M C, Haduch G A, Williams J B.A study to determine the effect of damping on finite-element-based, forced-frequency-response models for bottom hole assembly vibration analysis//65th SPE Annual Technical Conference and Exhibition, New Orleans, Louisiana. SPE-20458-MS.

[7]Asghar Jafari Ali, Kazemi Reza，Faraji Mahyari Mohammad. The effects of drilling mud and weight bit on stability and vibration of a drill string . Journal of Vibration and Acoustics, 2012, 01: 528-534.

[8]Gao Deli, Huang Wenjun. Some research advances in down hole tubular mechanics and control methods [J]. Advances in Mechanics, 2021, 51(03): 620-647.

[9]Zhang Hong, Xiang Zhengxin, Qian Liqin, et al. The correlation between the spindle load and the deflecting capacity of the wellbore trajectory control tool [J].Mechanics in Engineering, 2017, 39(2): 152-157,134.

[10]Zhang Hong, Feng Yijing, Xiang Zhengxin, et al. Study on Deformation Motion and Mechanical Model of the Shaft of the Wellbore Trajectory Control Tool[J]. Journal of Applied Science and Engineering, 2017, 20(4): 435-443.

[11]Zhang Guangwei, Hou Pengpeng, Li Junqiang, et al .Study on Vibration Characteristics of Guiding Shaft of New Directional [J]. Coal science and Technology, 2021, 49(10): 177-184.

[12]Zhang Guangwei, Hou Pengpeng, Cheng Liling, et al. Study on the dynamic characteristics of the joint bearing of a new directional rotary steering drilling tool [J]. Modern Manufacturing Engineering, 2020(11): 13-20.

[13]Zhang Guangwei, Qiao Yang, Tian Fan, et al. Dynamic analysis and simulation of full rotary built-in steering drilling tools[J]. Journal of Mechanical Strength, 2020, 42(06): 1417-1423.

[14]Wu qian. Research on operating characteristics of a new directional rotary steering spindle system [D].Chengdu: Southwest Petroleum University, 2018.

[15]Tian Weikang. A dynamic performance study on full rotation built-in tool guide mechanism[D]. Xi'an Shiyou University, 2017.

[16]Chen Yingjie, Fu Jianhong, Ma Tianshou, et al. Numerical Modeling of Dynamic Behavior and Steering Ability of a Bottom Hole Assembly with a Bent-Housing Positive Displacement Motor Under Rotary Drilling Conditions[J]. Energies 2018, 13(2):1-13.

[17]Jiang Shuyun，Zheng Shufei. A modeling approach for analysis and improvement of spindle-drawbar-bearing assembly dynamics[J]. International Journal of Machine Tools & Manufacture, 2010, 50(1): 131-142.
[18]Rui Xiaoting, Yun Laifeng, Lu Yuqi, et al. Transfer matrix method for multi body systems and its application. Beijing: Science press, 2008.
[19]Tang Bo, Wang Peng, Zhang Hong, et al. Study on Biasing force and Deflection Performance of Guiding Tool Spindles [J]. Mechanics in Engineering, 2022, 44(02):310-316.
[20]Tang Bo, Wang Peng, Zhang Hong, et al. Dynamic Characteristics of Eccentric Spindle of Guide Tool Based on Global Transfer Matrix Method [J]. Science Technology and Engineering, 2022, 22(19):8289-8294.
[21]Wang Bo,Sun Wei,Tai Xingyu,et al. The influence analysis of the dynamic characteristics of the spindle system on the spindle system[J]. Vibration and shock,2011,30(10):231-235.

Author contributions

F. D. put forward the research ideas.Z.H. and Z.Jx. wrote the main manuscript text.L.K. and L.Yj. conducted the experiment.All authors reviewed the manuscript.

Funding

Open Fund Project of the Technology Innovation Center for Directional Drilling Engineering, Ministry of Natural Resources(KF202402);Open Fund Project of the National Quality Inspection and Testing Center for Oil and Gas Drilling and Production Equipment (Hubei)(KF2023-Z001);Open Fund Project of the National Oil Production Equipment Engineering Technology Research Center of China(ZBKJ2024B-01).

Declarations

Competing interests

The authors declare no competing interests.

Additional information

Correspondence and requests for materials should be addressed to F.D.